Towards a dynamic fresnel zone model to WiFi-based human activity recognition

Jinyi Liu, Wenwei Li, Tao Gu, Ruiyang Gao, Bin Chen, Fusang Zhang, Dan Wu, Daqing Zhang

Towards a Dynamic Fresnel Zone Model to WiFi-based Human Activity Recognition

JINYI LIU, Peking University, China
WENWEI LI, Peking University, China
TAO GU, Macquarie Univerisity, Australia
RUIYANG GAO, ZEKU Technology, Co., Ltd, China
BIN CHEN, Lijiang culture and tourism college, China
FUSANG ZHANG, Institute of Software, Chinese Academy of Sciences and University of Chinese Academy of Sciences, China
DAN WU, Peking University, China
DAQING ZHANG*, Peking University, China and Telecom SudParis, France

The passive WiFi sensing research has largely centered on activity sensing using fixed-location WiFi transceivers, leading to the development of several theoretical models that aim to map received WiFi signals to human activity. Of these models, the Fresnel zone model has shown to be particularly noteworthy. However, the growing popularity of mobile WiFi receivers has not been matched by corresponding research on mobile receiver-based theoretical models. This paper fills this gap by presenting the first theoretical model to quantify the impact of moving a moving receiver for WiFi sensing. We propose a novel dynamic Fresnel zone model in the free space of an indoor environment, which takes the form of a cluster of concentric hyperbolas centered on the transmitter and reflection subject. We examine three properties of this model, i.e., relating the variation in RF signals received by the receiver to the position and orientation of the human, the movement of the receiver, and the presence of other objects in the environment. To validate this model, we develop a prototype system and conduct extensive experiments. The results are consistent with our theoretical analysis, and the system is able to detect the direction of the transmitter with an accuracy of 10° or better, measure the receiver's relative motion displacement within 1 *cm* a millimeter-level accuracy, and classify five receiver-side activities with an accuracy of 98%. Our work moves a significant step forward in WiFi sensing and may potentially open up new avenues for future research.

CCS Concepts: • **Computer systems organization** → **Embedded systems**; *Redundancy*; Robotics; • **Networks** → Network reliability.

*This is the corresponding author

Authors' addresses: Jinyi Liu, Peking University, Key Laboratory of High Confidence Software Technologies (Ministry of Education), School of Electronics Engineering and Computer Science, Beijing, China, liujinyi@pku.edu.cn; Wenwei Li, Peking University, Beijing, China; Tao Gu, Macquarie Univerisity, Department of Computing, Macquarie University, Sydney, Australia, tao.gu@mq.edu.au; Ruiyang Gao, ZEKU Technology, Co., Ltd, Beijing, China; Bin Chen, Lijiang culture and tourism college, Key Laboratory of High Confidence Software Technologies (Ministry of Education), School of Electronics Engineering and Computer Science, Beijing, China, dalichenbin@gmail.com; Fusang Zhang, Institute of Software, Chinese Academy of Sciences and University of Chinese Academy of Sciences, Beijing, China, 100190; Dan Wu, Peking University, Beijing, China; Daqing Zhang, Key Laboratory of High Confidence Software Technologies (Ministry of Education), School of Electronics Engineering and Computer Science, Peking University, Beijing, China , IP Paris and Telecom SudParis, Evry, France, dqzhang@sei.pku.edu.cn.

2474-9567/2023/6-ART65 $15.00
https://doi.org/10.1145/3596270

Additional Key Words and Phrases: Wireless sensing, Dynamic Fresnel Zone Model, Mobile Receiver, Channel state information, Dynamic Fresnel Zone Model

ACM Reference Format:
Jinyi Liu, Wenwei Li, Tao Gu, Ruiyang Gao, Bin Chen, Fusang Zhang, Dan Wu, and Daqing Zhang. 2023. Towards a Dynamic Fresnel Zone Model to WiFi-based Human Activity Recognition. *Proc. ACM Interact. Mob. Wearable Ubiquitous Technol.* 7, 2, Article 65 (June 2023), 24 pages. https://doi.org/10.1145/3596270

1 INTRODUCTION

Recent years have witnessed the emergence of a variety of mobile devices such as smartphones, tablets, and smartwatches that support WiFi communication, as WiFi-based wireless infrastructure has become widely available around the world. Built on this infrastructure, WiFi sensing has received increasing attention over the last decade. Based on the principle that humans affect the propagation of these signals, a typical scenario of WiFi sensing is to sense human activities in the setting of fixed-location WiFi transceivers. To understand the relationship between human activity and fluctuations in the received CSI signals, a series of theoretical models have been proposed, including the Fresnel zone[28][37], Fresnel diffraction model[45][47], and Sensing Coverage model[34]. These models have been developed to assist in characterizing the impact that human activities have on RF signals and to quantify the relationship between them. These models provide the theoretical basis for WiFi sensing when the transceivers are stationary, with various applications ranging from respiration monitoring [28, 41, 46], fall detection [30, 35], direction determination [37], localization [15, 29], to gesture recognition [1, 8, 9, 36].

Despite significant advancements in WiFi sensing, several new challenges have emerged that warrant further attention. One of the major limitations is that WiFi transceivers need to be placed at fixed locations in indoor scenarios. However, the proliferation of mobile communication devices such as smartphones and smartwatches has resulted in an increasing setting of mobile receiver. This has led to a new sensing scenario in which the transmitter is stationary but the receiver is mobile. The existing WiFi sensing model designed for stationary transceiver is hence unable to characterize the phenomena observed in this new scenario. Our preliminary experiments have revealed that the current WiFi sensing model is inadequate in explaining the complex interplay between the mobile receiver, signal propagation, and the surrounding environment. While some work has studied mobile WiFi receivers, the relationship between signal propagation and the receiver's location remains unknown and requires thorough investigation. Therefore, it is crucial to develop a deterministic perception model to quantitatively capture the relationship between signal propagation, receiver movement, and environmental factors, in order to inform system design and deployment decisions.

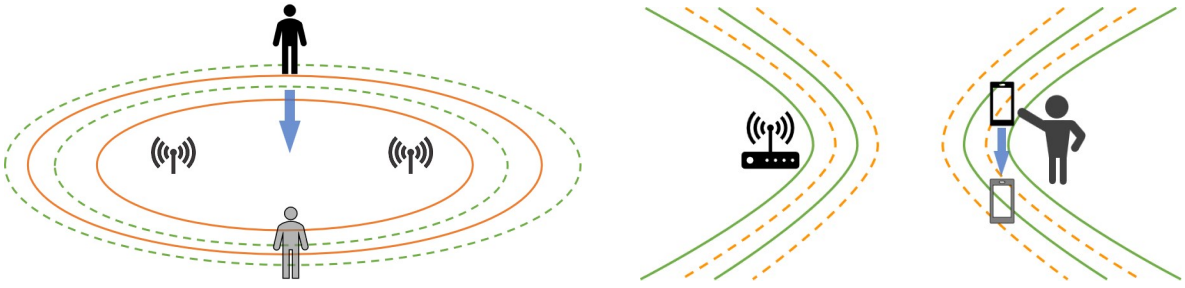

Fig. 1. The illustration of (a) the classic Fresnel zone model and (b) the dynamic Fresnel zone model.

The Fresnel zone model is a pivotal foundational framework in WiFi sensing that sheds light on the mechanisms of human activity sensing through wireless signals under stationary transceivers and provides the basis for most of the wireless sensing applications. As depicted in Fig.1(a), the Fresnel zone of WiFi signals encompasses a series of concentric ellipses with two foci in the fixed-location transceiver pair. This model assumes that the transceivers remains stationary while the human target moves in the Fresnel zone. When an object crosses a series of Fresnel zones, the received signal appears as a sin-like waveform, with peaks and valleys corresponding to the boundaries of the Fresnel zones. With the increasing prevalence of WiFi-enabled mobile devices, in this paper, we propose a dynamic Fresnel zone model that takes into account the mobility of WiFi receivers. We first examine the signal propagation characteristics in the absence of surrounding objects in the free space of an indoor environment and in the presence of a single reflection subject when the receiver is moving. Subsequently, we introduce the dynamic Fresnel zone model, which is a cluster of concentric hyperbolas with the transmitting antenna and the reflection serving as two focal points (as shown in Fig.1(b)). This model establish the relationship between the movement of the receiver and the received signal when the transmitter and the target are stationary, links the changes in the received signals to the location, distance, and orientation of a mobile receiver. Furthermore, we deploy the dynamic Fresnel zone model in an indoor environment and analyze its feasibility when multiple reflection subjects are present. Our theoretical analysis is substantiated by extensive experimental measurements.

Following the principle of the proposed sensing model, we develop a proof-of-concept prototype system using a pair of commodity WiFi devices. In a real-life scenario, the relative location of the transceiver pair is important for sensing. By applying the dynamic Fresnel zone model, our system is able to determine the relative orientation of the transmitter and the receiver. This is accomplished by controlling the movement of the receiver over a known distance in different directions of the dynamic Fresnel zone, with a median error of less than 10°. The distinctive hyperbolic density patterns of the dynamic Fresnel zone in different directions are utilized to achieve this goal. Once the relative orientation is established, the receiver can be used as a ruler. We can then calculate the moving distance of the receiver in 0-degree by counting the number of crossings of the dynamic Fresnel zone, with a margin of error of less than 1 cm. Finally, the system exploits the distinctive characteristics of the multi-carrier dynamic Fresnel zone to extract the stable features of carrier variability for each activity. Our experiments show that the system is able to reliably distinguish the five activities.

The main contributions of this work can be summarized as follows:

- This paper proposes a dynamic Fresnel zone model for the mobile receiver-based sensing scenarios and builds the theoretical foundation for WiFi sensing under mobile receiver conditions. The study extends the current WiFi sensing paradigm to mobile-receiver scenarios that encompass a wide range of mobile applications.
- From our in-depth analysis of signal propagation at mobile receivers in indoor environments, we develop a rigorous mathematical model that quantifies the relationship between RF signal variations and receiver-side activities. Through comprehensive experiments, we validate this model and uncover several unique features of a mobile receiver-based WiFi sensing system.
- Built on the dynamic Fresnel zone model, we present a proof-of-concept prototype system that is able to accurately detect receiver-side activities without knowing the relative locations of transceivers. Results show that the system achieves an activity recognition accuracy of 98%, an estimation error of the transmitter's angle within 10°, and an estimation error of the receiver's moving distance at the millimeter level.

The subsequent sections of this paper are organized as follows. In Section 2, we provide an overview of relevant prior work. Section 3 introduces the dynamic Fresnel zone model and its application to CSI signals. Section 4 outlines our approach for effectively utilizing the dynamic Fresnel zone model in the design of our system. The results of our experiments in real-life scenarios are presented in Section 5. We discuss the limitation of this work in Section 6, and the paper is concluded in Section 7.

2 RELATED WORK

This section discusses the most relevant works in three areas: Fresnel model-based human sensing, Non-WiFi-based gesture recognition, and WiFi-based gesture recognition.

2.1 Fresnel Zone Model-Based Human Sensing

The Fresnel zone is first used for human sensing by Wang et al.[28] and Wu et al.[37]. Wang et al.[28] first use the Fresnel zone to model activity sensing and build the relationship between the detectability of human respiration and human's orientation and location. Wu et al.[37] first detect human walking direction by the use of two orthogonal Fresnel zone with the use of two transceiver pairs, and they achieve a median error of less than 10 degrees. Zhang et al. [45] further examine the properties of the Fresnel reflection model for human sensing and determined its limitation. More recently, Wang et al.[29] and Liu et al.[17], focus on the impact of multipath on the Fresnel zone model, exploit ambient reflected CSI signals for indoor localization and respiration monitor. Zeng et al.[41] combine both CSI amplitude and phase in the Fresnel zone to achieve higher accuracy when human respiratory in different positions. Yang et. al. [39] and Zeng et.al. [42] use the Fresnel zone under multiple antennas to monitor respiration from multiple users [42]. However, the above works focused on the scenario where the subject is outside the Fresnel zone, therefore, it is also known as the Fresnel reflection model. Zhang et al. [47] [46] further study activity sensing inside the first Fresnel zone, and employ the Fresnel diffraction model to quantify the relationship between the diffraction gain and the location of the target.

During the past few years, the Fresnel zone has been extensively studied in depth, Gao et al.[8] describe the sensing quality of the signal, removing the location dependency of the Fresnel zone. Wang et al.[34] present that when the transmitter-receiver distance is further increased, the sensing area is separated from one ellipse into two ellipses located around the two transceivers. Niu et al.[21] investigate rigorously the dependency of velocity estimation accuracy on target locations and headings in the Fresnel zone.

2.2 Non-WiFi based Gesture Recognition

Non-RF gesture recognition mainly includes wearable-based, vision-based, and acoustic-based. Wearable-based systems require attaching wearable devices to the user's hand or arm to recognize gestures[38], Wearable ring-type [12] and watch-type sensors[27], are also utilized in human-computer interaction scenarios. Computer vision-based gesture recognition systems, such as Microsoft Kinect[18][19] and Leap Motion[14], rely on cameras or infrared sensors to capture human activity within the visual range and reconstruct the depth information of the images[44][7][23]. However, their performance can be greatly impacted by the illumination conditions. Acoustic-based gesture recognition approaches have also been used to recognize hand gestures by utilizing speakers and microphones[24][5][10][16]. LLAP [33] employs changes in the phase of acoustic signals for motion sensing, while FingerIO[20] employs OFDM-modulated acoustic signals for centimeter-level finger tracking and WiTrace[32] able to tracking centimeter-Level passive gesture. However, the limited sensing range of acoustic waves restricts its usage. Chen et al.[6] also use LTE Terminals for robust hand gestures.

2.3 WiFi-based Gesture recognition

In recent years, the utilization of WiFi signal measurements such as CSI and RSSI have been widely used for gesture recognition [3][26][40]. By employing multiple antennas or receiving devices, this approach uses radio frequency signals to track the movements of a hand and determine their distance and velocity. Despite these advancements, these systems still present certain limitations. For example, RF-IDraw [31] utilizes an RFID tag attached to a glove and achieves a tracking accuracy of 5.5 cm, WiDraw [25] can track the user's hand with a median error lower than 5 cm yet its operating range is limited to less than 2 feet and multiple antennas are required. Wideo [13] necessitates the use of an antenna array with an average positioning error of 0.8 m.

QGesture [40], on the other hand, attains a hand tracking accuracy of 5.5 cm through the utilization of rough phase information obtained from a commercially available WiFi device.

Different from existing work, we exploit the dynamic Fresnel zone model for mobile WiFi receivers. The proposed dynamic Fresnel zone model quantifies the relationship between the receiver's movement controlled by the subject and the path length change of obtained CSI signal. We believe this model complements to existing Fresnel zone model, creating more possibilities for the perception of mobile devices.

3 UNDERSTANDING DYNAMIC FRESNEL MODEL

In this section, we first introduce the basic principles of the dynamic Fresnel zone model when there is only one reflection target in the free space of an indoor environment, and then analyze the characteristics of the multi-carrier dynamic Fresnel zone. Following this, we design a series of experiments to verify the dynamic Fresnel zone and derive its three properties. Finally, we examine the influence of other reflection target when there is more than one surrounding subject in the indoor environment.

3.1 Preliminary

The Fresnel zones are concentric ellipses as shown in Fig.2, where P1 and P2 represent a pair of stationary RF signal transceivers, while the Fresnel zone containing n layers is constructed as follows:

$$|P_1Q_n| + |Q_nP_2| - |P_1P_2| = n\lambda/2 \tag{1}$$

where Q_n is the point of the n th layer of ellipses, the length of the reflected path $P_1Q_1P_2$ is $n\lambda/2$ wavelengths longer than the linear propagation path P_1P_2. When an object crosses a series of Fresnel zones, the received signal appears as a sin-like waveform, with peaks and valleys corresponding to the boundaries of the Fresnel zones[28][45].

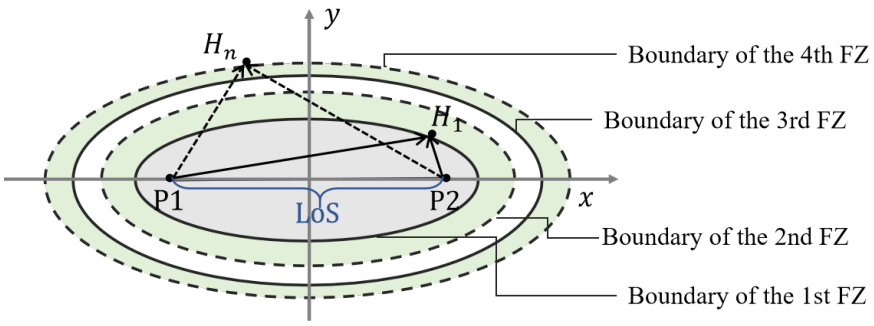

Fig. 2. Geometry of the Fresnel Zone

3.2 The Basic of Dynamic Fresnel Model

When the transceiver pair is located in free space or open environment without ambient reflection signal exists, the received CSI signal is only related to the change of direct path between transceiver pair, which can be written as:

$$H(f_i, t) = A(t)e^{-j2\pi f_i \frac{d(t)}{c}} \tag{2}$$

where $e^{-j2\pi f_i \frac{d(t)}{c}}$ is the phase shift of received CSI, A, $d(t)$, f_i and c are the complex attenuation, propagation length, frequency of the i th sub-carrier and the velocity of light, respectively. In the case of a stationary transmitter

and mobile receiver, the received CSI signal is only related to the change of the direct path between transceivers when the transceiver pair is located in free space or an open environment without ambient reflection subject exists.

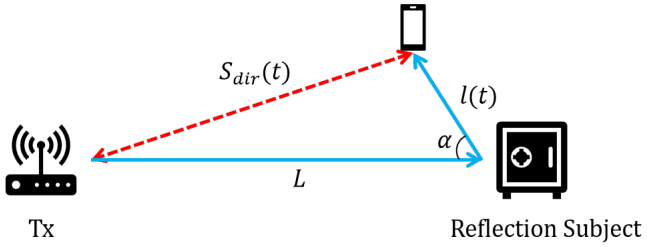

Fig. 3. Presentation of the one surrounding subject scenario.

However, there may be fewer cases in which no static subject exists in a real-life environment. Whenever the receiver moves, there is usually at least one reflection subject presented, e.g., the person holding the receiver. As shown in Fig.3, when there is only one stationary surrounding subject in the environment, the signal received from the mobile receiver is composed of two parts of propagation: the direct path, which propagates directly from the transmitter (illustrated in red line), and the reflected path, which reflects through the subject (illustrated in blue line). CSI obtained can be presented as:

$$H(f_i,t) = H_1(f_i,t) + H_2(f_i,t) = A_1(t)e^{-j2\pi f_i \frac{S_{dir}(t)}{c}} + A_2(t)e^{-j2\pi f_i \frac{L+l(t)}{c}} \tag{3}$$

where $H_1(f_i,t)$ and $H_2(f_i,t)$ present the component of direct path and reflected path, $S_{dir}(t)$ and $L + l(t)$ are the path length of each component, respectively.

Accordingly, the length between the transmitter and reflection subject $|TxP|$ remains unchanged when the receiver moves with a stationary reflection subject, while the path length of direct signal $|TxR_n|$ and reflected signal from the target to transmitter $|PR_n|$ are both changes with receiver movement. In the context of radio propagation, the distance between the direct path and reflected path determines the difference in phase [11], Despite the fact that the path length of the reflected signal $|TxPR_n|$ is λ longer than the path length of the direct signal $|TxR_n|$, there is a phase difference of 2π between the two signals, which indicates that the superimposed signal is stronger. When the distance between two paths is $\lambda/2$, the phase difference is π, and the two signal amplitudes are reversed, the superimposed received signals cancel each other out. We can write the difference between the two paths as follows:

$$|TxP| + |PR_n| - |TxR_n| = L + l(t) - S_{dir}(t) = n\lambda/2 \tag{4}$$

Inspired by the definition of hyperbola, where for any point of P on the hyperbola set, the absolute difference of the distances $|PF_1|, |PF_2|$ to two stationary points F_1,F_2 (the foci) is constant. Inspired by the definition of the Fresnel zone model, we construct the dynamic Fresnel model as the concentric hyperbola with two foci in the transmitter Tx and static surrounding subject P by ensuring:

$$||TxR_n| - |PR_n|| = ||TxP| - n\lambda/2| \tag{5}$$

where R_n is a point on the nth hyperbola.

As shown in Fig.4, the innermost hyperbola close to the transmitter and the stationary subject (two foci) is defined as the 1st dynamic Fresnel zone, the hyperbola curve between the first hyperbola and the second is defined as the 2nd dynamic Fresnel zone, and the nth dynamic Fresnel zone corresponds to the hyperbola curve between the $(n-1)$th and nth hyperbola. However, in the dynamic Fresnel zone model the number of hyperbolic

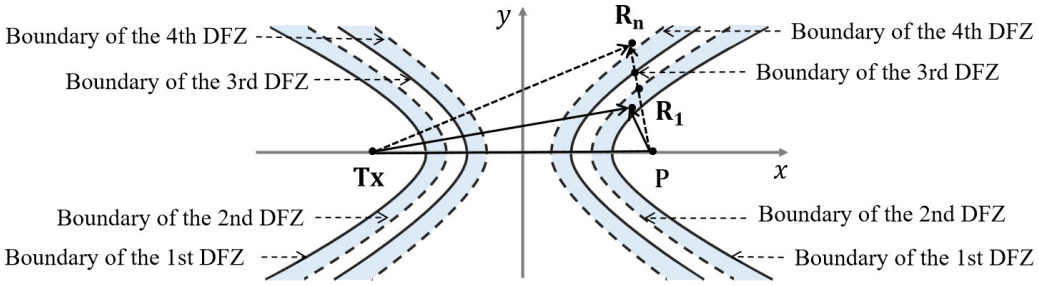

Fig. 4. Geometry of the Dynamic Fresnel Zone

clusters is limited by the distance between the transmitter and surrounding subject, i.e. $|TxP| <= n\lambda/2$ and $n <= 2|TxP|/\lambda$ accordingly. We further define the boundary of the nth dynamic Fresnel zone as the hyperbola between nth and $(n+1)$th dynamic Fresnel zones:

$$b_n = \{(R_n, Tx, P) \quad ||TxP| + |PR_n| - |TxR_n|| = n\lambda/2(n <= 2|TxP|)\} \tag{6}$$

Apparently, when an object moves from the first Fresnel zone to the nth Fresnel zone, the phase difference between the direct and reflected path signals increases as the object moves outward through the different Fresnel zones. According to the basic interference principle, when the object crosses the boundary of the Fresnel zone, the received signal appears as a peak or a valley. However, if the object moves along a hyperbola, the received signal remains unchanged because the difference between the length of the reflected and direct signal paths does not change.

Based on the analysis above, it is easy to obtain the first property of WiFi RF propagation with the mobile receiver as follows:

- **P1**: WiFi dynamic Fresnel zones take the shape of concentric hyperbolas with two foci in the transmitter and reflection subject which can be calculated mathematically.

3.3 Impact of Receiver's Moving Direction

As can be seen from the above analysis, the density of hyperbolic clusters differs in different directions, so when the receiver moves in the same direction along different directions, the phase change of the received signal differs; For a better understanding of the relationship between the activity direction of the receiver and the phase change of received signal, as presented in Fig.4 we assume that the receiver is moving in the direction of α from the line connecting of transmitter and reflection subject (two foci) at a distance of TxP, the variation in the path difference lengths of the reflected and direct paths can be expressed as:

$$\begin{aligned} \Delta D = |S_{ref}(t) - S_{dir}(t)| &= |TxP| + |PR_n| - \sqrt{|PR_n|^2 \sin^2\alpha + (|TxP| - |PR_n|\cos\alpha)^2} \\ &= |TxP| + |PR_n| - \sqrt{(|TxP| - |PR_n|)^2 + 4|TxP||PR_n|\sin^2\frac{\alpha}{2}} \end{aligned} \tag{7}$$

It can be seen that, when $\alpha = 0$, $\Delta D = 2|TxP|$, in this case, the phase change caused by the movement of the receiver is only affected by the moving distance, independent of the distance between the transmitter and the reflection subject. As α increases, ΔD and phase change of received RF signal decrease correspondingly. Thus we can obtain the second property of the dynamic Fresnel model as fellow:

- **P2**: The phase change caused by a receiver movement on a line between the transmitter and the reflection subject is only related to the receiver movement distance.

3.4 Impact of Frequency Diversity

In this section, we devote to taking full use of the frequency diversity of the dynamic Fresnel zone. So far, we introduced the main properties of the dynamic Fresnel zone model, we can see that, when the receiver is located at the boundary of the dynamic Fresnel zone, the direct and reflected paths differ by an integer multiple of half the wavelength ($\lambda/2$). Currently, we can measure the CSI of 30 or 52 subcarriers in most commercial WiFi devices, each of which has its own wavelength and frequency. In WiFi signals, each channel has a stationary center frequency, e.g. 5.24 GHz, and different sub-carriers are distributed around this center frequency at equal intervals of $\Delta f = 312.5\,kHz$ in 802.11n and 802.11ac. Therefore, we can further describe the multi-carrier Fresnel zone model as follows:

$$b_n = \{(R_n, T, P) \quad ||TxP| + |PR_n| - |TxR_n|| = n\lambda_i/2(n <= 2|TxP|)\} \tag{8}$$

where λ_i is wavelength of ith subcarrier, it can be seen that even though the receiver is in the same position, the Fresnel zone differs for different subcarriers, e.g., when R_n is at the boundary of the mth Fresnel zone for the 1st subcarrier, it may be between the mth and $(m+1)$th Fresnel zones for the Nth subcarrier.

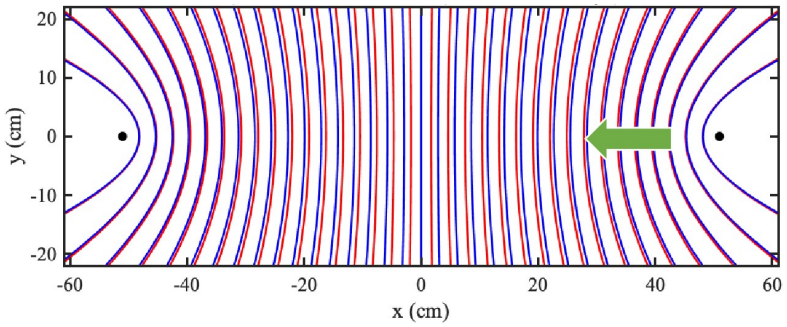

Fig. 5. Dynamic Fresnel zone for both the head and tail subcarriers.

For a better understanding of the dynamic Fresnel model under frequency diversity, we consider the two extreme subcarriers $f_1 = 5.24\,GHz$ and $f_2 = f_1 + 51 \times \Delta f$ with wavelengths λ_1 and λ_2. As illustrated in Fig.5, we simulate the dynamic Fresnel zone model with the frequency of f_1 (line in red) and f_2(line in blue), respectively. It can be seen that these two subcarriers almost overlap their inner dynamic Fresnel zones boundaries and the difference between their corresponding zone boundaries keeps increasing as the number of zones increases until the boundary of the ith Fresnel zone of f_m catches up with $(i+1)$th Fresnel zone of subcarrier f_n. Let c be the speed of light, the phase difference $\Psi(f_1, f_2)$ between two subcarriers can be written as:

$$\Psi(f_1, f_2) = \frac{2\pi f_1 |L_D - L_R|}{c} - \frac{2\pi f_2 |L_D - L_R|}{c} = \frac{2\pi \Delta F \Delta L}{c} \tag{9}$$

where L_D, L_R present the path length of the direction signal and the reflected signal, respectively. From the analysis above, we can see that the difference between subcarriers increases when the receiver moves from the inner dynamic Fresnel zone to the outer dynamic Fresnel zone, when the receiver approaches the inner dynamic Fresnel zone, the carrier discrepancy decreases.

Thus we can obtain the third property of the dynamic Fresnel zone model:

- **P3**: As the receiver moves away from and closer to the inner Fresnel region, the subcarrier variability of the received signal increases and decreases accordingly.

3.5 Verification with Benchmark Experiments

In this section, we verify the existence of WiFi dynamic Fresnel Zone in an indoor environment through experiments. As shown in Fig.6, the verification experiments are conducted in an office room with less multipath to better visualize the above properties. We use a metal cup with a diameter of 30 cm and a height of 19 cm as the reflection subject. The transmitter and metal cup are placed 3 m apart with 42 cm height, to precisely control the displacement of the receiver, we mount it on a high-precision linear motion slider with an accuracy of 0.01 mm. Transmitter (Tx) and receiver (Rx) both use one omnidirectional vertically-polarized antenna. The central frequency is 5.24 GHz, which corresponds to 5.725 cm wavelength. The initial distance between the receiver and the metal cup is 12 cm, as the receiver moves along the slider, the length of both the direct and reflected path changes accordingly.

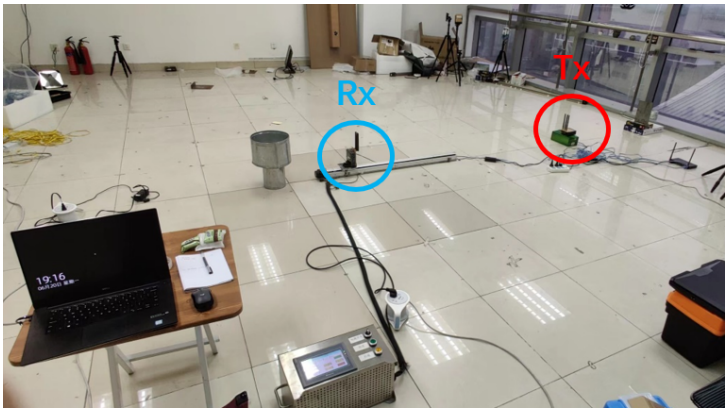

Fig. 6. The experimental environment and deployment of transceivers.

3.5.1 Verification of P1. To verify the shape of the dynamic Fresnel zone, as shown in Fig.7(a), we first draw the concentric hyperbolic curves, the boundaries of Fresnel zones are colored in blue and red, indicating the odd and even Fresnel zones respectively. Note that, for better presentation, this is only a schematic. For the purpose of verifying the existence of the dynamic Fresnel zone, we move the receiver along 3 different degrees with the same 50 cm. We first move the receiver along the perpendicular bisector (0-degree) from 4 th to 22 th Fresnel zone. We expect to observe 17 valleys and 17 peaks presented alternately, where the first one should be a valley as a result of crossing the boundary of the 4 th Fresnel zone. To verify that WiFi Fresnel zones are concentric hyperbolic curves, we control the receiver to move along three paths at the same distance, as shown in Fig.7(a). The paths were labeled 0-degree, 45-degree, and 90-degree. For each of these three paths, we should observe 17, 15, and 8 peaks, corresponding to the number of zone boundaries crossed.

From the above experiment we can see that: (1) The occurrence sequence of valleys and peaks match the index of the dynamic Fresnel model. (2) A concentric hyperbolic curve with foci at the transmitter and surrounding subjects explains the occurrence time and the number of valleys/peaks for each path correctly. (3) A continuous sine wave appears when the receiving signal crosses a series of dynamic Fresnel zones, confirming the expected phase change.

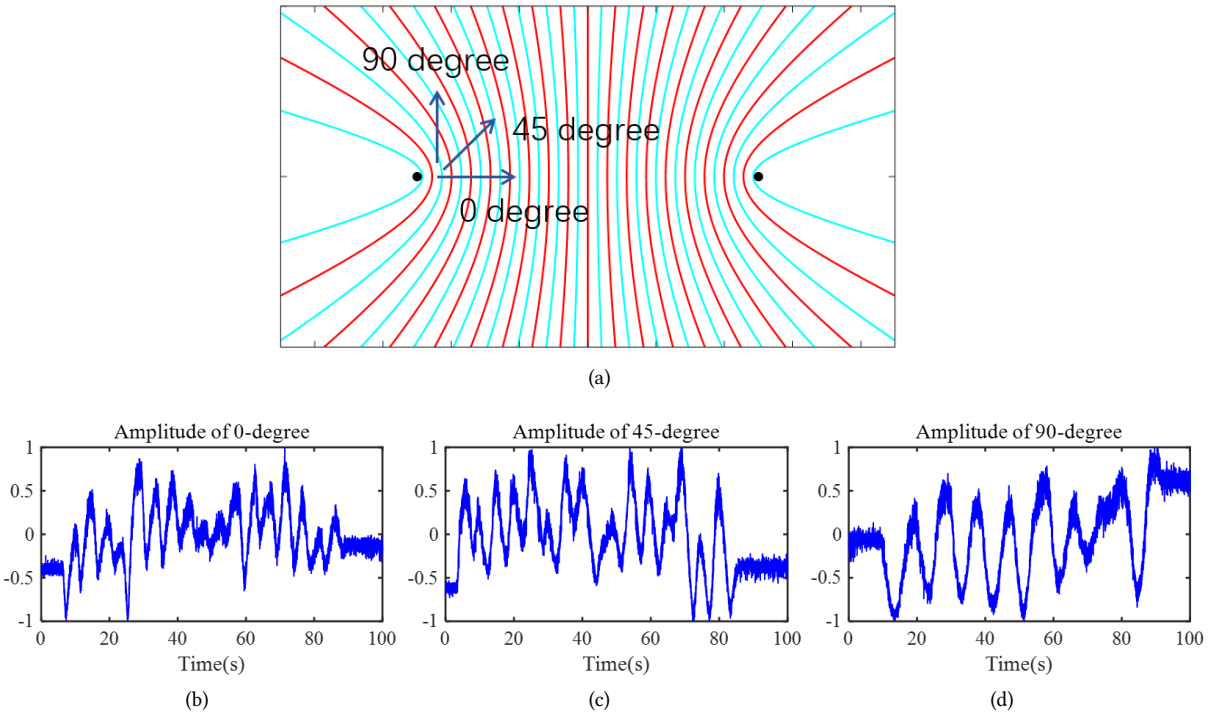

Fig. 7. Dynamic Fresnel zone experimental settings (up) and results (down): (b) 0-degree, (c) 45-degree, (d) 90-degree.

3.5.2 Verification of P2. To verify the phase change when the receiver moves along the perpendicular bisector (0-degree, on a line between transmitter and surrounding subject). We fix the moving orientation and control the receiver to move along 20 cm at 0-degree, and change the relative position of the transmitter in each experiment, the distance between the transmitter to the reflection subject is 2.4 m, 3.6 m, and 4.2m, respectively.

By theoretical calculation, we should observe 6 valleys/peaks in each experiment. Fig.8 presents the CSI amplitude received from each scenario, the same sine-like waveform was obtained in each experiment, as expected.

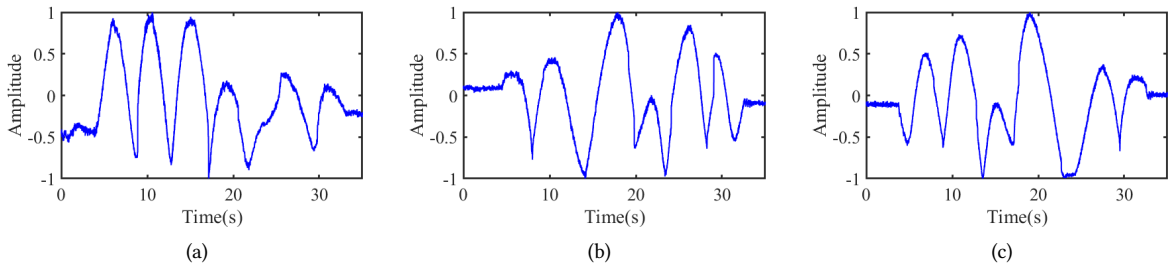

Fig. 8. Received CSI amplitude when the distance between surrounding subject and transmitter is: (a) 2.4m, (b) 3.6m, (c) 4.2m.

3.5.3 Verification of P3. As shown in Fig.5, we control the receiver to move from the inner dynamic Fresnel zone to the outer. Based on our theoretical analysis, the consistency of different subcarriers tends to decrease over time. Fig.9 shows the CSI amplitude from different subcarriers with idx=1, idx=15, and idx=30, respectively. We can see that with the receiver moving outward, the position of each peak/valley from different subcarriers is gradually dispersed, i.e., the first wave crests appear in different carriers at almost the same time, but by the time it reaches the 4 th peak, there is an obvious sequence.

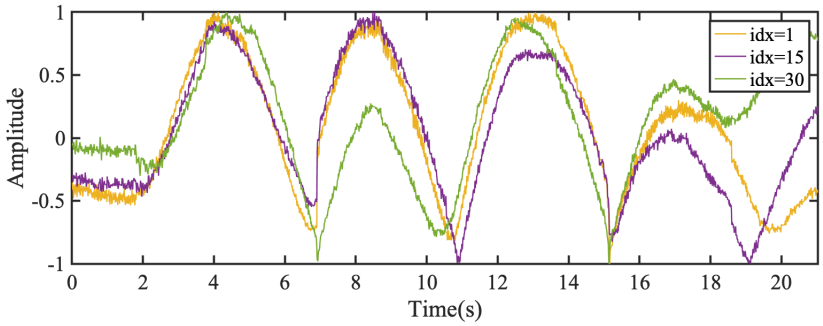

Fig. 9. CSI amplitude from 1 st, 15 th, and 30 th subcarrier when the receiver moves away from the inner dynamic Fresnel zone.

To sum up, these benchmark experiments validate the three properties of the dynamic Fresnel zone model, the experimental results match the theoretical plots very well. These three properties relate the phase change from the mobile receiver to the dynamic Fresnel zone, and discover the nature and scope of the dynamic Fresnel zone. According to the previous study, the human body is always modeled as a varying-size semi-cylinder[28, 42, 43, 46], which means that the human body can be considered as a surrounding subject when a person is standing. Consequently, activity associated with a mobile receiver can be viewed as moving through a dynamic Fresnel zone with the transmitter as the two foci point. With the dynamic Fresnel zone model, we are able to sense the motion of the receiver via WiFi signals.

3.6 Impact of Surrounding Subjects

We have already discussed the dynamic Fresnel zone model when there exists one reflection subject. Nevertheless, in real life, there is always more than one static subject in the surrounding environment. As an example, when a person holds a receiver during an activity, the received signal includes the reflected signal from the human target as well as the reflected signal from other static objects, e.g., walls, furniture, etc. As the title suggests, this section will discuss the effects of multiple reflection subjects on the dynamic Fresnel zone.

We first take the example of two surrounding subjects in the environment as presented in Fig.10, where $P1$ and $P2$ represent the two surrounding subjects, respectively, and the receiver is moving along the red line, close to $P1$. It can be seen that the received signal contains a direct signal from the transmitter and reflected signals from the two reflected subjects, respectively. In this state, the received signal consists of the direct signal and reflection signal from two reflection subjects:

$$H(f,t) = H_D(f,t) + H_{R1}(f,t) + H_{R2}(f,t) = A_S(t)e^{-j2\pi f\frac{D(t)}{c}} + A_{P1}(t)e^{-j2\pi f\frac{S_1+d_1(t)}{c}} + A_{P2}(t)e^{-j2\pi f\frac{S_2+d_2(t)}{c}} \quad (10)$$

where $H_D(f,t)$, $H_{R1}(f,t)$ and $H_{R2}(f,t)$ present CSI received from the transmitter and two reflection subjects, respectively, A_S, A_{P1} and A_{P2} is the amplitude power of each path. As shown in Fig.10, $D(t)$ presents the length

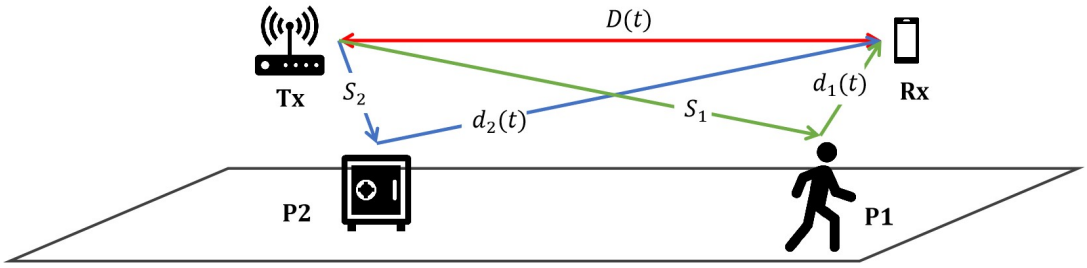

Fig. 10. Presentation of Two Surrounding Subjects Scenario

of the direct path, S_1, S_2 is the distance between the transmitter and each surrounding subject, $d_1(t), d_2(t)$ present the reflected path length from two surrounding subjects to the receiver, respectively. Without loss of generality, we can divide the direct signal into two parts: the equation above can be written as:

$$H(f,t) = \frac{A_S(t)A_{P1}}{A_{P1}+A_{P2}} e^{-j2\pi f \frac{D(t)}{c}} + A_{P1}(t)e^{-j2\pi f \frac{S_1+d_1(t)}{c}} + \frac{A_S(t)A_{P2}}{A_{P1}+A_{P2}} e^{-j2\pi f \frac{D(t)}{c}} + A_{P2}(t)e^{-j2\pi f \frac{S_2+d_2(t)}{c}} \tag{11}$$

In this case, the received signal can be viewed as a superposition of two dynamic Fresnel zones, with transmitter-P1 and transmitter-P2 as two foci points. Furthermore, the received signal can be considered as a superposition of the signals received from each dynamic Fresnel zone. In accordance with the wave superposition principle, when two electromagnetic waves of different frequencies are superimposed, the synthesized wave has the same number of peaks and valleys as the high-frequency electromagnetic wave. We apply Fourier transform to superimposed CSI, obtaining the strongest frequency-domain component representing the dynamic Fresnel zone with transmitter-P1 foci points. This method is used in real scenarios for CSI components conforming to our dynamic Fresnel model.

We verify the effect of other surrounding subjects by placing new reflectors at different locations around the receiver. In this experiment, we use another metal cup with a diameter of 36 cm and a height of 19 cm as the second surrounding subject. As illustrated in Fig.11, the distance between the transmitting terminal and the first reflection point P1 is 2 m, the second surrounding subject P2 is placed perpendicular to P1, and the straight-line distance is 0.8m, the receiver moves 30 cm in a 45°, with the Initial distance of 12 cm from P1. In this scenario, the distance from the second surrounding subject to the receiver is always larger than that from the first surrounding subject to the receiver.

Fig.11(b) shows the CSI amplitude obtained when there is only one surrounding subject P1 located in the environment, and Fig.11(c) illustrates the CSI amplitude obtained with the influence of both P1 and P2. It can be seen that the peaks/valleys' number of the obtained amplitude of both scenarios is the same, in good agreement with the theoretical plots.

4 GUIDING SYSTEM DESIGN FOR RECEIVER'S ACTIVITY

In this section, we design a sensing system for mobile receiver leveraging on our proposed model in Section 3. Based on the mobile-receiver-based properties, the dynamic Fresnel zone model is able to guide the system which supports the following three different functions: (1)Estimation of transmitter orientation; (2)Distance measurement for the receiver; (3)Classify the activity trajectory of human subject;

4.1 System Overview

First, our system can assist the user in determining the relative direction of the transceiver pair, i.e., when the user does not know where the transmitter is, our system can determine its relative orientation with greater precision.

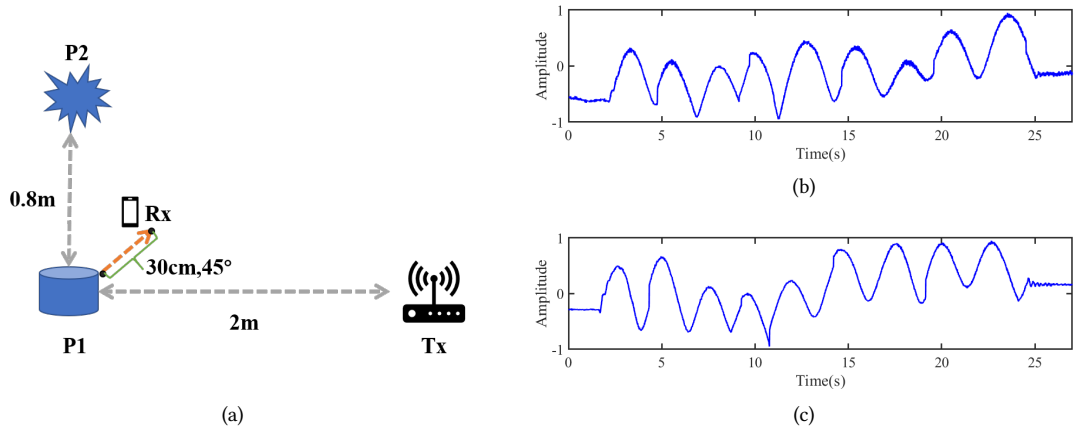

Fig. 11. Experiment setup in a real-life scenario (a), CSI amplitude obtain when there is only one surrounding subject (P1) (b) and two neighboring surrounding subjects P1 and P2.

Then, our system can be viewed as a ruler. When the direction of the transmitter is known, we can measure the moving distance of the receiver via the received CSI signal when it moves along 0-degree. Finally, guided by the multi-carrier dynamic Fresnel zone, our system is able to classify five underlying activity trajectories of receiver.

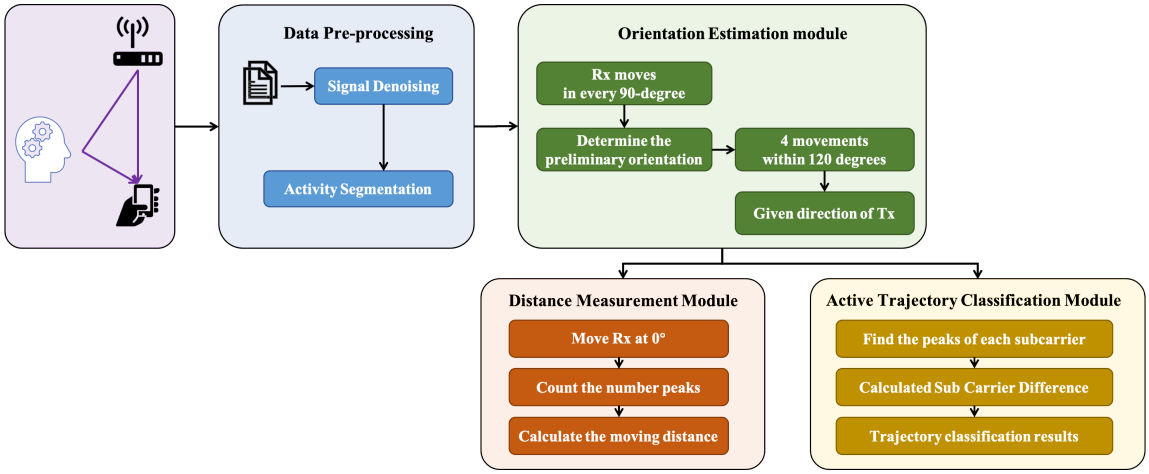

Fig. 12. System Overview

As illustrated in Fig.12, our system begins with data acquisition and pre-processing, which takes raw Channel State Information (CSI) readings gathered from commodity Wi-Fi receivers as input. In this step, we adopt the Savitzky-Golay filter[22] to process the noisy raw signal. Note that, S-G filtering is also widely used as a denoise method in the pre-processing step of existing WiFi sensing systems. Then, our system works in three parts, corresponding to the three applications mentioned above. The orientation estimation module estimates the relative orientation of the transceiver pair via the property of the dynamic Fresnel zone. The distance measurement

module estimates the moving distance of the receiver by calculating the peaks/valleys of the received CSI signal. The active trajectory classification module classifies the active trajectories of common receivers by the variability of the performance of different trajectories in the multi-carrier Fresnel zone.

4.2 Orientation Estimation Module

This section examines how to guide the estimation of transmitter orientation via the dynamic Fresnel zone. From the properties we summarized before, we can see that the sensing of the mobile receiver in the dynamic Fresnel zone is orientation-dependent, i.e., when a person faces in different directions and holds the receiver move the same distance, the peaks/valleys obtained from CSI amplitude are different. Our system is designed to determine the relative orientation of the transmitter by moving the receiver the same distance in different directions when the transmitter's position is unknown. According to Fig.13, in order to accomplish this goal, we move the receiver at every 90 degrees, and from this activity, we can determine the approximate orientation of the receiver. For more precise orientation information, we move the same distance at another 30 or 40-degree interval within 120-degree around that direction, as shown in the right part of Fig.13, and from this, we can determine the exact transmitter end orientation.

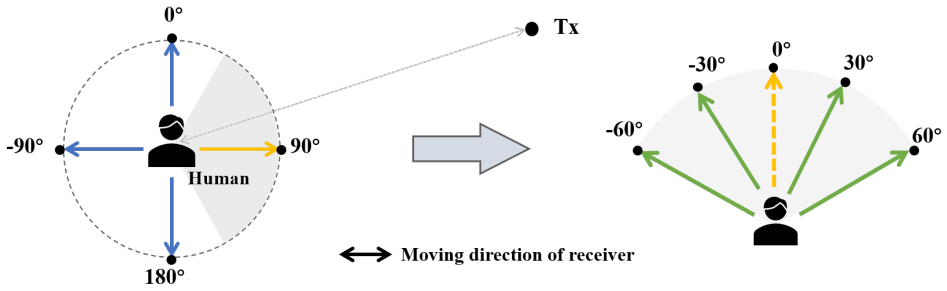

Fig. 13. Two steps for orientation estimation.

According to our experiments, it is difficult to control hands to move the same distance in different directions and to ensure that each movement is precisely spaced by 90° or 30°. As a solution to this problem, we use the IMU sensors available in handheld WiFi devices (e.g., smartphones) to assist our judgment. We refer to the IMU trajectory reduction algorithm proposed in the existing system[4] and obtain the trajectory and relative angle of the smartphone.

After determining the precise distance and angle of each movement of the receiver, we are able to calculate the number of traversed dynamic Fresnel zones by counting the number of peaks and valleys obtained from CSI amplitude. Based on the characteristics of the dynamic Fresnel zone, it can be determined that the receiver traverses the more dynamic Fresnel zones when it is active on the line between the transmitter and the human target, we can assume the approximately direction of the transmitter. By comparing the results obtained in the second step at different orientations, combining with the dynamic Fresnel zone model, we can calculate a precise result, which is almost the same as the actual value. The real-life experimental results are presented in Section 5.2.

4.3 Distance Measurement Module

Based on our analysis in Section 3.3, when the receiver moves on the line between the transmitter and the human target, the obtained CSI signal only relates to the moving distance of the receiver. Therefore, at this point, the

phase change of the received signal is not affected by the distance between the transmitter and the surrounding subject, regardless of how far away the transmitter is.

Once we obtain the relative orientation of the transmitter, we can use the above characteristic of the dynamic Fresnel zone to measure the moving distance of the receiver on the transceiver link. Equation 7, in particular, can be used to determine the relative distance of the receiver activity by calculating the number of peaks in the received CSI amplitude. That is to say, each dynamic Fresnel zone traversed is reflected as a peak in the CSI amplitude, and the corresponding distance of the receiver increases or decreases by $\lambda/2$. When a total of N peaks are received at the receiver, the relative distance of activity at the receiver can be computed as $N \times \lambda/2$. The detailed experimental results are presented in Section 5.3.

4.4 Activity Trajectory Classification Module

In Section 3.4, we analyze the property of the multi-carrier dynamic Fresnel zone and give an example in Fig. 9 to illustrate that different sub-carriers behave differently when the receiver is active from the inner dynamic Fresnel zone to the outer dynamic Fresnel zone. The system is intended to use the x-axis symmetry of the dynamic Fresnel zone and its characteristics under multi-carrier to classify the active trajectory of human subject via moving receiver. According to the properties of dynamic Fresnel zones, the receiver should be held directly opposite the transmitter end in order to achieve better perceptual repeatability. With the help of the above two modules, we are able to obtain a more accurate relative angle of the transmitter. This module addresses the design of multiple robustly identifiable trajectory.

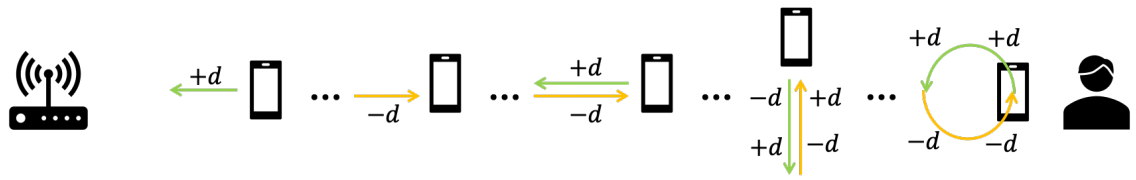

Fig. 14. Five movements we recognized: forward, backward, forward and backward, left and right, and drawing circle.

As illustrated in Fig.14, this system aims to recognize five realistic and commonly used movements, i.e. forward, backward, forward and backward, left and right, and drawing circle. According to the analysis in Section 3.4, we can observe that, when the receiver is moving forward, the discrepancy between subcarriers becomes larger, and when the receiver is moving backward, the discrepancy between subcarriers becomes smaller. As the receiver moves left and right, the subcarrier discrepancy becomes smaller and then larger, and it is smallest at the crossing of the transmitting end and the surrounding subject. For two subcarriers, we characterize the subcarrier discrepancy by the difference in time Δt_n between their appearance of the nth wave peak/valley.

As illustrated in Fig.14, we define the signal variation patterns of five trajectories via the use of subcarrier discrepancy. By using the symbol +, we indicate that the subcarrier discrepancy increases when the receiver moves the same distance d, and by using the symbol −, we indicate that it decreases. When the receiver is moved away from the human target, the corresponding pattern of signal variability is indicated by $+d$. In the same manner, other unique signal change patterns may also be defined, such as drawing circles as $+d + d - d - d$, etc. Fig.15 shows the CSI amplitudes received by two subcarriers with $\Delta idx = 29$ when the receiver is drawing circle, the pattern $+d + d - d - d$ can be observed obviously. By this way, we can achieve highly accurate of activity trajectory recognition by mapping well-defined signal change patterns to different trajectory types without training. Trajectories for receiver-side movement can also be recognized to provide a new means of human-computer interaction. Real-life experiments are presented in Section 5.4. However, it is important to

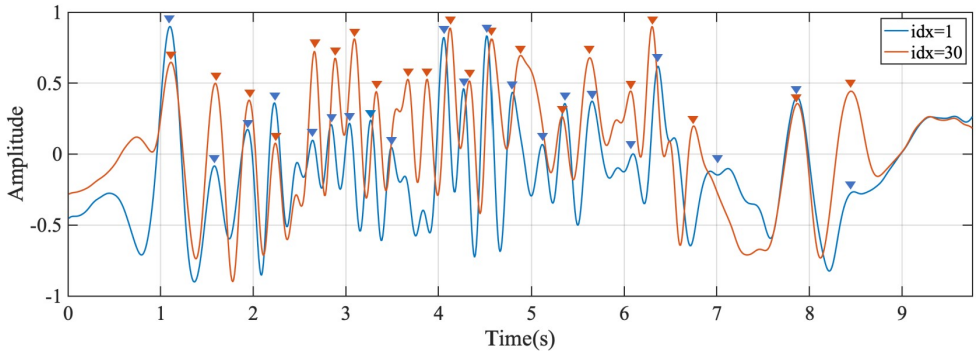

Fig. 15. CSI amplitude from two different subcarrier when the receiver act as drawing circle.

note that the performance of our algorithm may deduce in different scenarios especially in multi-path rich environment (mobile receiver close to surrounding objects). In the future, we will continue to further improve this algorithm.

5 EVALUATION

To evaluate the performance of the proposed mobile receiver-based sensing model, we conduct comprehensive experiments to evaluate its performance. We first describe the system setup for data collection and then present the results for each module from a series of experiments.

5.1 Experimental Settings

We use a pair of commercial WiFi 6 network cards provided by AICSemiconductor [2], as illustrated in Fig.16(a) and (b), each WiFi card is equipped with one antenna. The transmitter operates at a central frequency of 5.24 GHz with a bandwidth of 40 MHz and broadcasts 100 packets per second. We directly collect CSI data from the receiver and process the data in MATLAB using a DELL Precision 5520 laptop (Intel Xeon E3-1505M v6 CPU and 8 GB RAM). In general, we are able to obtain 52 sub-carriers from the receiver.

We recruit 8 volunteers (i.e., 3 males and 5 females), aged from 14 to 58 years old. We conducted experiments in relatively quiet environments with less interference, including a conference room, an office, a hallway, and a residential apartment which consists of two bedrooms, one living room, one study room, and one bathroom. We collect a total of more than 120 hours of data for our experiments. The ground truth of the receiver's moving distance and trajectory is collected by the IMU sensors installed in Samsung's Galaxy 4, we use the continuous strokes reconstructed method proposed in [4] to obtain the trajectory.

5.2 Estimate the Direction of Transmitter in LoS Scenario

Experiments are conducted in three different environments, as shown in Fig.16(c-e), for each environment, we ask the subject to stand or sit on the chair with the receiver held in hand. As presented in Fig.17(a), the transmitter is placed with 5 different positions, and the distance between each position is 1 meter. The distance between the transmitter and the human target (i.e. denoted as S in Fig.17(a).) is ranged from 2.5 m-5.5 m, at a step size of 1 m. As introduced in Section 4.2, the subject is first asked to move the receiver every 90 degrees in the same distance and then move 4-5 times within 120 degrees around that approximate orientation we select.

We define an error as the absolute value of the difference between the transmitter's orientation we calculate and the true angle in real-life. Fig. 17(b) shows the confusion matrix of mean error. It can be seen that as the

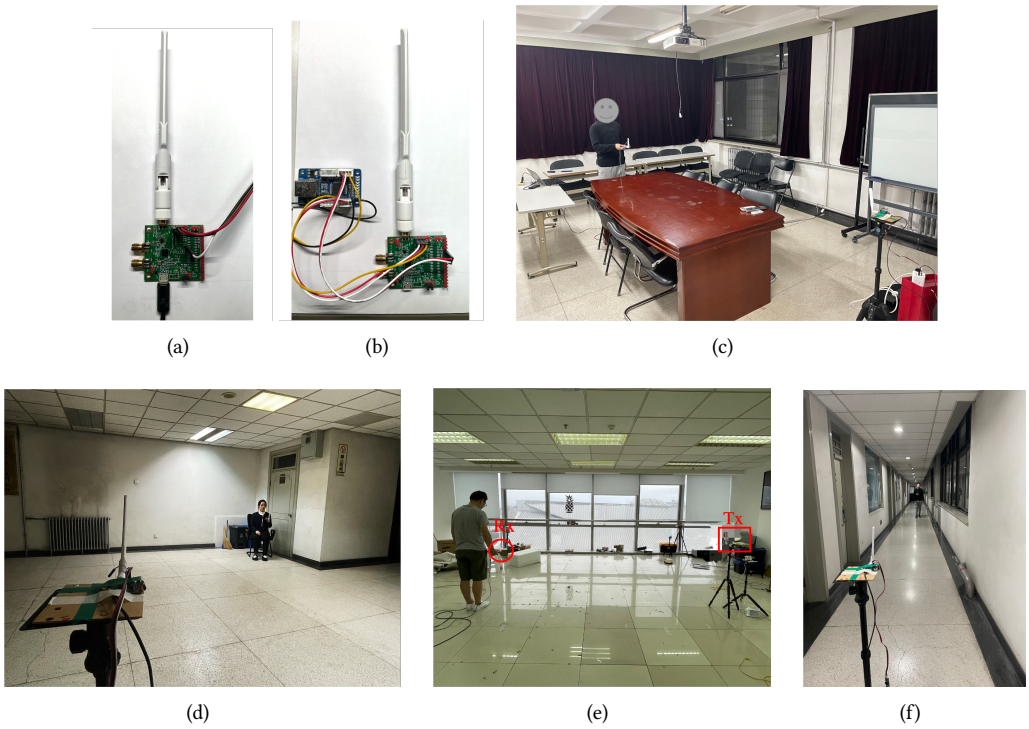

Fig. 16. The WiFi (a)transmitter, (b)receiver and (c-f) different experiment setups we used in this work.

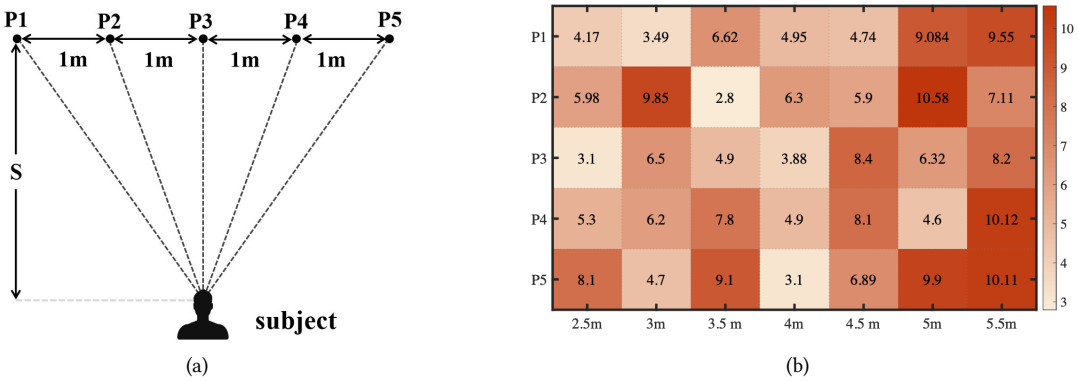

Fig. 17. The illustration of (a) transmitter's orientation and (b) confusion matrix.

distance between the transmitter and the person becomes larger, the error increases, which we believe is the reason for the larger signal noise at the receiver. The result reveals that the maximum mean error is 11 degrees.

This means that our system provides a good estimation of the transmitter side direction in different scenarios using a transceiver pair.

5.3 Measure the Moving Distance of Receiver in 0-degree

In this experiment, we focus on the second module of our system, evaluating the performance of 1 D distance measurement with a transceiver pair. As shown in Fig.16(f), the experiment is conducted in a corridor, and the distance between the subject and the transmitter is varied from 2 m to 10 m at a step size of 1 m. At each distance, we ask the subject to move the receiver in his hand in the direction of the transmitter randomly.

We evaluate the performance with absolute displacement error, which is defined as $|D_{est} - D_{gt}|$, where D_{est} is the estimated receiver displacement and D_{gt} is the ground truth obtained by IMU. Further, we classify the obtained CSI signal by the moving distance of the receiver, i.e., less than 10 cm, 10 cm-20 cm, 20 cm-30 cm, 30 cm-40 cm, and more than 40 cm. As shown in Fig. 18, the mean error of absolute displacement for each of the above cases is less than 1 cm, demonstrating the distance measuring capability of our system. It can be seen that the average error growing up with the receiver's moving distance, we believe this is due to the fact that some volunteers are unable to keep the receiver moving straightly towards the transmitter a longer distance.

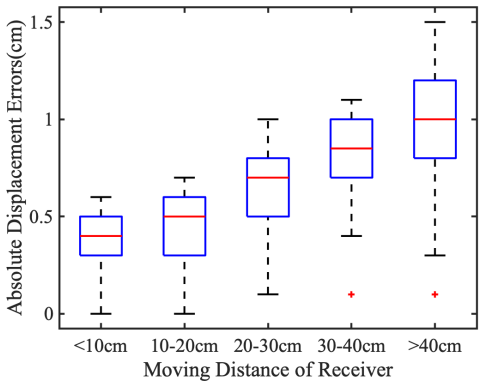

Fig. 18. The absolute displacement error.

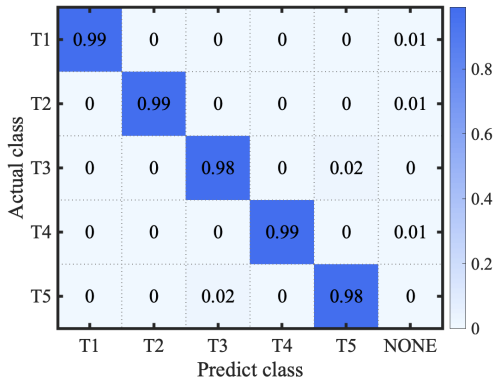

Fig. 19. Confusion Matrix of trajectory classification.

5.4 Classify the Trajectory of Mobile Receiver

We focus on verifying the third module of our system in this experiment. Experiments are conducted in the same scenarios in Fig.16(c-e), the distance between transmitter and volunteers is from 2.5 m to 5.5 m. We collect samples from three different scenarios with five users. Each user was asked to face the transmitter and perform every trajectory 20 times (i.e., 10 times for both right and left hand) in each scenario at a different time. Note that, the volunteers do not move the receiver in a certain size, through our observations, we find that the moving size of the receiver varied between 10 cm-60 cm, the moving size here refers to the distance moved forward and backward or left and right, as well as the diameter of the drawing circle.

Fig.19 shows the confusion matrix of the classification accuracy, where T1-T5 present forward, backward, forward and backward, left and right, and drawing circle, respectively. It can be seen that our system can achieve high performance with an average recognition accuracy of 98.2%. Fig.20(a) shows the overall results with different transmitter-subject distance in a different environment. It can be seen that, different environments and static

multi-paths have very little impact on accuracy. In our proposed recognition scheme, it is reasonable to assume that it is designed to combat ambient noise and make the system robust in a variety of environments.

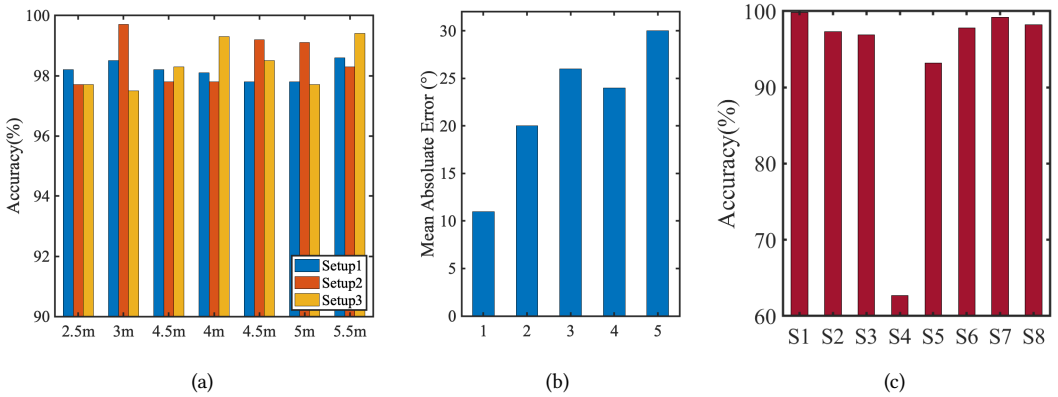

Fig. 20. The performance in (a) different scenario, (b) challenging scenario and (c) extra surrounding subject.

To investigate the impact of the distance between the receiver and the wall. We conduct experiments in the scenario shown in Fig.21(a). Specifically, we place the transmitter 30 cm away from the wall and the vertical distance between the human subject and the transmitter is 3m. We ask volunteers to stand at distances ranging from 30 cm to 4 m apart from the wall, facing the transmitter, to evaluate the performance of our system in recognizing five different trajectories of mobile receiver. Additionally, as illustrated in Fig.21(b), we ask volunteers to move the receiver with three different sizes: large (50 cm-60 cm), medium (30 cm-40 cm), and small (10 cm-20 cm). It is important to note that the moving size here refers to the distance moved forward and backward or left and right, as well as the diameter of the drawing circle.

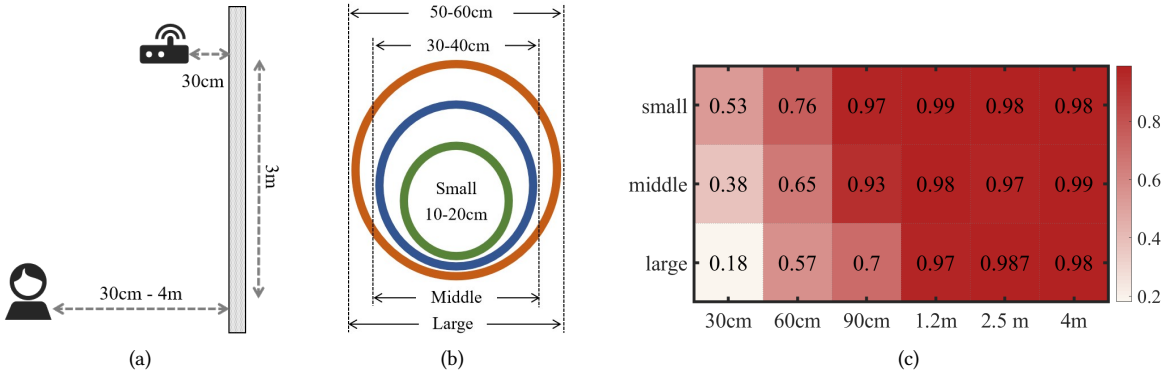

Fig. 21. The illustration of (a) the subject's different distances from the wall (b) three different sizes of the movements and (b) performance of trajectory classification.

Fig.21(c) displays the overall recognition performance of five different trajectories of mobile receiver under different moving displacement and distances from the wall. It can be seen that when a subject moves the receiver

at a distance of more than 1.2 m from the wall, the accuracy is not affected. When a subject is within 1 m from the wall, the closer the subject comes to the wall, the worse the accuracy becomes. Additionally, the smaller the range of movement of the receiver is, the better the recognition performance we achieve. We believe that this is because when a subject is closer to the wall, the distance between the receiver and the wall during movement is less than the distance between the receiver and the subject. This observation is consistent with the analysis of surrounding subjects in Sec.3.6.

5.5 Performance in Challenging Scenario

In this subsection, we evaluate the performance of our system in challenging scenarios, the experiment is set up in a real residential apartment that consists of two bedrooms, one living room, one study room, and one bathroom. We put the transmitter in a different room from the receiver with a wall in between. As presented in Fig.22, the subject is located in the study room, and the transmitter is placed in different rooms, namely setups 1, 2, 3, 4, and 5, for each setup, there exists a wall in between the receiver which blocks the Line-of-Sight (LoS). Fig.20(b) shows the mean orientation error given by the system in each setup. It should be noted that the exact original orientation between transmitter and receiver is hard to obtain due to the complex structure and furniture in the apartment, so we can only estimate a relative angle. It can be seen that the angular errors we calculate are all within 30 degrees, at which point it is possible to successfully point out the room where the transmitter is located.

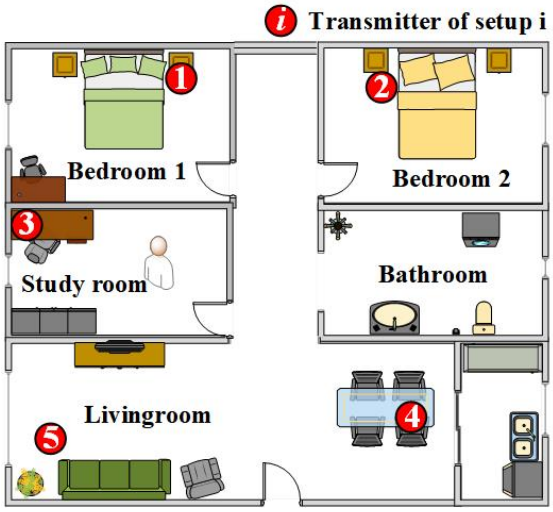

Fig. 22. Experiment setup in the residential apartment.

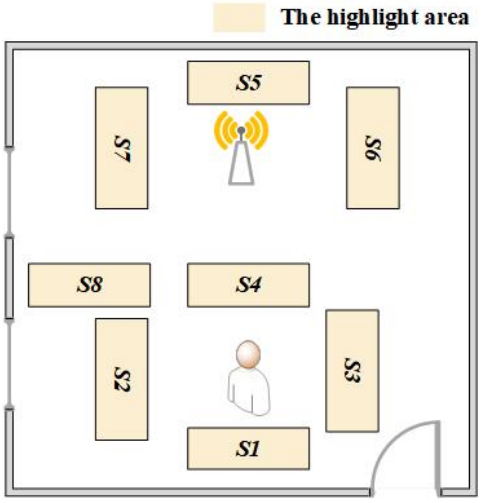

Fig. 23. Experiment settings for investigation of surrounding subjects.

5.6 Impact of Ambient Reflection

To study the effect of ambient reflection, i.e., the reflected signal from other static objects in the environment, we conduct additional experiments in a large office room (7.5 m × 9 m) as shown in Fig.23. We further vary the distance between the transmitter and the subject from 2 m to 5 m at a step size of 1 m. We place static reflectors in each of the eight highlighted areas (i.e., the areas indicated by $S1 - S8$). Note that when the receiver is moving, only the distance between the $S4$ and the receiver is larger than the distance between the subject and the receiver.

The experimental results show that when the other subject stays or moves far away from the transceiver pair, the ambient reflection can be tolerated. As presented in Fig.20(c) when there exists a static object in $S4$ or other areas around the receiver, the classification result of the activities' trajectory drop to around 60%, when it exists far from both transmitter and receiver, the result is unaffected. To a certain degree, when the distance between the motion and the transceivers increases, the performance is improved.

6 DISCUSSION AND LIMITATION

In this section, we discuss the limitations of this work and suggest potential directions for future work.

Impact of surrounding subjects: In the dynamic Fresnel zone model, we assume that the human target is the nearest object in proximity of the mobile receiver. However, if there are multiple objects nearby, recognition accuracy may decrease. Therefore, it is crucial to consider environmental factors when deploying the system and to ensure that the receiver is positioned in a more open space to minimize the impact of the surrounding environment. By doing so, we can improve the recognition accuracy of the system and enhance its overall performance.

The non Line-of-Sight (NLoS) scenario: We observe that the proposed dynamic Fresnel zone model works under the LoS scenario, which requires full visibility between the transceivers and the human target. However, when the direct path between the transmitter and receiver is blocked, the signal may reach the receiver through multiple reflections or bypassing, which can significantly affect the accuracy.

Comparison with stationary transceiver pairs: Our extensive experiments reveal that in contrast to the standard Fresnel zone model, the dynamic Fresnel zone model designed for the mobile receiver scenario has the advantage of a larger sensing range, e.g., when we increase the distance between the transceiver pair to 8m, the signal obtained from the stationary scenario is submerged in noise, making it difficult to observe clear signal change patterns via raw CSI amplitude. However, in the mobile scenario, the signal change patterns corresponding to three different hand gestures are clear.

Multiple transceiver pairs: Our analysis of the dynamic Fresnel zone model is currently based on a transceiver pair. For future work, we plan to extend our study to multiple transceiver pairs to fully explore its potential. Additionally, we aim to combine this model with the existing Fresnel zone model that uses stationary transmitters, which will enable wider application scenarios. We will also use multiple antennas to further improve the performance. It is worth noting that while this paper focuses on applying our theory to WiFi sensing, it can be applied to other RF-based sensing in general.

7 CONCLUSION

This paper advances WiFi sensing by proposing the first theoretical model of the dynamic Fresnel zone in free space, characterized by a cluster of concentric hyperbolas with foci at the transmitter and surrounding subject. We validate the dynamic Fresnel zone model through extensive experiments in indoor environments, examining the relationship between RF signal variations and human position, receiver's moving direction, multi-subcarriers, and the presence of other objects. The results of these experiments are surprising and provide insight into the impact of moving receivers on RF signals. By utilizing this sensing model, we are able to detect the direction of the transmitter with a median error of around 10 degrees, measure the receiver's moving distance at vertical angles with a millimeter-level accuracy, and classify 5 common receiver trajectories with an accuracy rate above 98%. We believe the methodology presented in this study fills a gap in the existing theoretical studies of WiFi sensing based on Fresnel zones and understand wireless sensing at a deeper level.

ACKNOWLEDGMENTS

This work is partially supported by the National Natural Science Foundation of China A3 Foresight Program (No.62061146001), the PKU-NTU Collaboration Project, the National Natural Science Foundation of China (No.62172394), the Beijing Natural Science Foundation (L223034), the Beijing Nova Program, the Youth Innovation Promotion Association, Chinese Academy of Sciences (No. 2020109).

REFERENCES

[1] Heba Abdelnasser, Moustafa Youssef, and Khaled A. Harras. 2015. WiGest: A ubiquitous WiFi-based gesture recognition system. In *2015 IEEE Conference on Computer Communications (INFOCOM)*. 1472–1480. https://doi.org/10.1109/INFOCOM.2015.7218525

[2] aicsemi. [n.d.]. aicsemi. https://www.aicsemi.com/sy.

[3] Kamran Ali, Alex X. Liu, Wei Wang, and Muhammad Shahzad. 2015. Keystroke Recognition Using WiFi Signals *(MobiCom '15)*. Association for Computing Machinery, New York, NY, USA, 90–102. https://doi.org/10.1145/2789168.2790109

[4] Yanling Bu, Lei Xie, Yafeng Yin, Chuyu Wang, Jingyi Ning, Jiannong Cao, and Sanglu Lu. 2022. Handwriting-Assistant: Reconstructing Continuous Strokes with Millimeter-Level Accuracy via Attachable Inertial Sensors. *Proc. ACM Interact. Mob. Wearable Ubiquitous Technol.* 5, 4, Article 146 (dec 2022), 25 pages. https://doi.org/10.1145/3494956

[5] Ke-Yu Chen, Daniel Ashbrook, Mayank Goel, Sung-Hyuck Lee, and Shwetak Patel. 2014. AirLink: Sharing Files between Multiple Devices Using in-Air Gestures. In *Proceedings of the 2014 ACM International Joint Conference on Pervasive and Ubiquitous Computing* (Seattle, Washington) *(UbiComp '14)*. Association for Computing Machinery, New York, NY, USA, 565–569. https://doi.org/10.1145/2632048.2632090

[6] Weiyan Chen, Kai Niu, Deng Zhao, Rong Zheng, Dan Wu, Wei Wang, Leye Wang, and Daqing Zhang. 2020. Robust Dynamic Hand Gesture Interaction using LTE Terminals. In *19th ACM/IEEE International Conference on Information Processing in Sensor Networks, IPSN 2020, Sydney, Australia, April 21-24, 2020*. IEEE, 109–120. https://doi.org/10.1109/IPSN48710.2020.00017

[7] Xiang 'Anthony' Chen, Julia Schwarz, Chris Harrison, Jennifer Mankoff, and Scott E. Hudson. 2014. Air+touch: Interweaving Touch amp; in-Air Gestures *(UIST '14)*. Association for Computing Machinery, New York, NY, USA, 519–525. https://doi.org/10.1145/2642918.2647392

[8] Ruiyang Gao, Wenwei Li, Yaxiong Xie, Enze Yi, Leye Wang, Dan Wu, and Daqing Zhang. 2022. Towards Robust Gesture Recognition by Characterizing the Sensing Quality of WiFi Signals. *Proceedings of the ACM on Interactive, Mobile, Wearable and Ubiquitous Technologies* 6, 1 (2022), 1–26.

[9] Ruiyang Gao, Mi Zhang, Jie Zhang, Yang Li, Enze Yi, Dan Wu, Leye Wang, and Daqing Zhang. 2021. Towards Position-Independent Sensing for Gesture Recognition with Wi-Fi. *Proceedings of the ACM on Interactive, Mobile, Wearable and Ubiquitous Technologies* 5, 2 (2021), 1–28.

[10] Sidhant Gupta, Daniel Morris, Shwetak Patel, and Desney Tan. 2012. SoundWave: Using the Doppler Effect to Sense Gestures. In *Proceedings of the SIGCHI Conference on Human Factors in Computing Systems* (Austin, Texas, USA) *(CHI '12)*. Association for Computing Machinery, New York, NY, USA, 1911–1914. https://doi.org/10.1145/2207676.2208331

[11] H. D. Hristov. 2000. Fresnel Zones in Wireless Links, Zone Plate Lenses and Antennas. *Artech House, Inc.* (2000).

[12] Lei Jing, Yinghui Zhou, Zixue Cheng, and Tongjun Huang. 2012. Magic Ring: A Finger-Worn Device for Multiple Appliances Control Using Static Finger Gestures. *Sensors (Basel, Switzerland)* 12 (2012), 5775 – 5790.

[13] Kiran Joshi, Dinesh Bharadia, Manikanta Kotaru, and Sachin Katti. 2015. WiDeo: Fine-grained Device-free Motion Tracing using RF Backscatter. In *12th USENIX Symposium on Networked Systems Design and Implementation (NSDI 15)*. USENIX Association, Oakland, CA, 189–204. https://www.usenix.org/conference/nsdi15/technical-sessions/presentation/joshi

[14] leapmotion. [n.d.]. leapmotion. https://www.leapmotion.com/.

[15] Xiang Li, Daqing Zhang, Qin Lv, Jie Xiong, Shengjie Li, Yue Zhang, and Hong Mei. 2017. IndoTrack: Device-free indoor human tracking with commodity Wi-Fi. *Proceedings of the ACM on Interactive, Mobile, Wearable and Ubiquitous Technologies* 1, 3 (2017), 1–22.

[16] Kang Ling, Haipeng Dai, Yuntang Liu, and Alex X. Liu. 2018. UltraGesture: Fine-Grained Gesture Sensing and Recognition. In *2018 15th Annual IEEE International Conference on Sensing, Communication, and Networking (SECON)*. 1–9. https://doi.org/10.1109/SAHCN.2018.8397099

[17] J. Liu, Y. Zeng, T. Gu, L. Wang, and D. Zhang. 2021. WiPhone: Smartphone-based Respiration Monitoring Using Ambient Reflected WiFi Signals. *Proceedings of the ACM on Interactive Mobile Wearable and Ubiquitous Technologies* 5, 1 (2021), 1–19.

[18] Giulio Marin, Fabio Dominio, and Pietro Zanuttigh. 2014. Hand gesture recognition with leap motion and kinect devices. In *2014 IEEE International Conference on Image Processing (ICIP)*. 1565–1569. https://doi.org/10.1109/ICIP.2014.7025313

[19] Mirosoft. [n.d.]. *Kinect*. http://www.microsoft.com/en-us/kinectforwindows/

[20] Rajalakshmi Nandakumar, Vikram Iyer, Desney Tan, and Shyamnath Gollakota. 2016. FingerIO: Using Active Sonar for Fine-Grained Finger Tracking. In *Proceedings of the 2016 CHI Conference on Human Factors in Computing Systems* (San Jose, California, USA) *(CHI '16)*. Association for Computing Machinery, New York, NY, USA, 1515–1525. https://doi.org/10.1145/2858036.2858580

[21] Kai Niu, Xuanzhi Wang, Fusang Zhang, Rong Zheng, Zhiyun Yao, and Daqing Zhang. 2022. Rethinking Doppler Effect for Accurate Velocity Estimation With Commodity WiFi Devices. *IEEE J. Sel. Areas Commun.* 40, 7 (2022), 2164–2178. https://doi.org/10.1109/JSAC.2022.3155523

[22] Ronald W. Schafer. 2011. What Is a Savitzky-Golay Filter? [Lecture Notes]. *IEEE Signal Processing Magazine* 28, 4 (2011), 111–117. https://doi.org/10.1109/MSP.2011.941097

[23] Jie Song, Gábor Sörös, Fabrizio Pece, Sean Ryan Fanello, Shahram Izadi, Cem Keskin, and Otmar Hilliges. 2014. In-Air Gestures around Unmodified Mobile Devices. In *Proceedings of the 27th Annual ACM Symposium on User Interface Software and Technology* (Honolulu, Hawaii, USA) *(UIST '14)*. Association for Computing Machinery, New York, NY, USA, 319–329. https://doi.org/10.1145/2642918.2647373

[24] Ke Sun, Ting Zhao, Wei Wang, and Lei Xie. 2018. VSkin: Sensing Touch Gestures on Surfaces of Mobile Devices Using Acoustic Signals. In *Proceedings of the 24th Annual International Conference on Mobile Computing and Networking* (New Delhi, India) *(MobiCom '18)*. Association for Computing Machinery, New York, NY, USA, 591–605. https://doi.org/10.1145/3241539.3241568

[25] Li Sun, Souvik Sen, Dimitrios Koutsonikolas, and Kyu-Han Kim. 2015. WiDraw: Enabling Hands-Free Drawing in the Air on Commodity WiFi Devices. In *Proceedings of the 21st Annual International Conference on Mobile Computing and Networking* (Paris, France) *(MobiCom '15)*. Association for Computing Machinery, New York, NY, USA, 77–89. https://doi.org/10.1145/2789168.2790129

[26] Sheng Tan and Jie Yang. 2016. WiFinger: Leveraging Commodity WiFi for Fine-Grained Finger Gesture Recognition. In *Proceedings of the 17th ACM International Symposium on Mobile Ad Hoc Networking and Computing* (Paderborn, Germany) *(MobiHoc '16)*. Association for Computing Machinery, New York, NY, USA, 201–210. https://doi.org/10.1145/2942358.2942393

[27] Tran Huy Vu, Archan Misra, Quentin Roy, Kenny Choo Tsu Wei, and Youngki Lee. 2018. Smartwatch-Based Early Gesture Detection 8 Trajectory Tracking for Interactive Gesture-Driven Applications. *Proc. ACM Interact. Mob. Wearable Ubiquitous Technol.* 2, 1, Article 39 (mar 2018), 27 pages. https://doi.org/10.1145/3191771

[28] Hao Wang, Daqing Zhang, Junyi Ma, Yasha Wang, Yuxiang Wang, Dan Wu, Tao Gu, and Bing Xie. 2016. Human respiration detection with commodity wifi devices: do user location and body orientation matter?. In *Proceedings of the 2016 ACM International Joint Conference on Pervasive and Ubiquitous Computing*. 25–36.

[29] Hao Wang, Daqing Zhang, Kai Niu, Qin Lv, Yuanhuai Liu, Dan Wu, Ruiyang Gao, and Bing Xie. 2017. MFDL: A multicarrier Fresnel penetration model based device-free localization system leveraging commodity Wi-Fi cards. *arXiv preprint arXiv:1707.07514* (2017).

[30] Hao Wang, Daqing Zhang, Yasha Wang, Junyi Ma, Yuxiang Wang, and Shengjie Li. 2017. RT-Fall: A Real-Time and Contactless Fall Detection System with Commodity WiFi Devices. *IEEE Transactions on Mobile Computing* 16, 2 (2017), 511–526. https://doi.org/10.1109/TMC.2016.2557795

[31] Jue Wang, Deepak Vasisht, and Dina Katabi. 2014. RF-IDraw: Virtual Touch Screen in the Air Using RF Signals. *SIGCOMM Comput. Commun. Rev.* 44, 4 (aug 2014), 235–246. https://doi.org/10.1145/2740070.2626330

[32] Lei Wang, Ke Sun, Haipeng Dai, Wei Wang, Kang Huang, Alex X. Liu, Xiaoyu Wang, and Qing Gu. 2021. WiTrace: Centimeter-Level Passive Gesture Tracking Using OFDM Signals. *IEEE Transactions on Mobile Computing* 20, 4 (2021), 1730–1745. https://doi.org/10.1109/TMC.2019.2961885

[33] Wei Wang, Alex X. Liu, and Ke Sun. 2016. Device-Free Gesture Tracking Using Acoustic Signals. In *Proceedings of the 22nd Annual International Conference on Mobile Computing and Networking* (New York City, New York) *(MobiCom '16)*. Association for Computing Machinery, New York, NY, USA, 82–94. https://doi.org/10.1145/2973750.2973764

[34] Xuanzhi Wang, Niu Kai, Jie Xiong, Bochong Qian, Zhiyun Yao, Tairong Lou, and Daqing Zhang. 2022. Placement Matters: Understanding the Effects of Device Placement for WiFi Sensing. *Proceedings of the ACM on Interactive, Mobile, Wearable and Ubiquitous Technologies* 6 (03 2022), 1–25. https://doi.org/10.1145/3517237

[35] Yuxi Wang, Kaishun Wu, and Lionel M. Ni. 2017. WiFall: Device-Free Fall Detection by Wireless Networks. *IEEE Transactions on Mobile Computing* 16, 2 (2017), 581–594. https://doi.org/10.1109/TMC.2016.2557792

[36] Dan Wu, Ruiyang Gao, Youwei Zeng, Jinyi Liu, Leye Wang, Tao Gu, and Daqing Zhang. 2020. FingerDraw: Sub-wavelength Level Finger Motion Tracking with WiFi Signals. *IMWUT* 4, 1 (2020), 31:1–31:27. https://doi.org/10.1145/3380981

[37] Dan Wu, Daqing Zhang, Chenren Xu, Yasha Wang, and Hao Wang. 2016. WiDir: walking direction estimation using wireless signals. In *Proceedings of the 2016 ACM international joint conference on pervasive and ubiquitous computing*. 351–362.

[38] Jiahui Wu, Gang Pan, Daqing Zhang, Guande Qi, and Shijian Li. 2009. Gesture Recognition with a 3-D Accelerometer, Vol. 5585. 25–38. https://doi.org/10.1007/978-3-642-02830-4_4

[39] Yanni Yang, Jiannong Cao, Xuefeng Liu, and Kai Xing. 2018. Multi-person sleeping respiration monitoring with COTS WiFi devices. In *2018 IEEE 15th International Conference on Mobile Ad Hoc and Sensor Systems (MASS)*. IEEE, 37–45.

[40] Nan Yu, Wei Wang, Alex X. Liu, and Lingtao Kong. 2018. QGesture: Quantifying Gesture Distance and Direction with WiFi Signals. *Proc. ACM Interact. Mob. Wearable Ubiquitous Technol.* 2, 1, Article 51 (mar 2018), 23 pages. https://doi.org/10.1145/3191783

[41] Youwei Zeng, Dan Wu, Ruiyang Gao, Tao Gu, and Daqing Zhang. 2018. FullBreathe: Full Human Respiration Detection Exploiting Complementarity of CSI Phase and Amplitude of WiFi Signals. *Proceedings of the ACM on Interactive, Mobile, Wearable and Ubiquitous Technologies* 2, 3 (2018), 148.

[42] Youwei Zeng, Dan Wu, Jie Xiong, Jinyi Liu, Zhaopeng Liu, and Daqing Zhang. 2020. MultiSense: Enabling multi-person respiration sensing with commodity wifi. *Proceedings of the ACM on Interactive, Mobile, Wearable and Ubiquitous Technologies* 4, 3 (2020), 1–29.

[43] Youwei Zeng, Dan Wu, Jie Xiong, Enze Yi, Ruiyang Gao, and Daqing Zhang. 2019. Farsense: Pushing the range limit of wifi-based respiration sensing with csi ratio of two antennas. *Proceedings of the ACM on Interactive, Mobile, Wearable and Ubiquitous Technologies* 3, 3 (2019), 1–26.

[44] Chi Zhang, Josh Tabor, Jialiang Zhang, and Xinyu Zhang. 2015. Extending Mobile Interaction Through Near-Field Visible Light Sensing. In *Proceedings of the 21st Annual International Conference on Mobile Computing and Networking* (Paris, France) *(MobiCom '15)*. Association for Computing Machinery, New York, NY, USA, 345–357. https://doi.org/10.1145/2789168.2790115

[45] Daqing Zhang, Hao Wang, and Dan Wu. 2017. Toward centimeter-scale human activity sensing with Wi-Fi signals. *Computer* 50, 1 (2017), 48–57.

[46] Fusang Zhang, Kai Niu, Jie Xiong, Beihong Jin, Tao Gu, Yuhang Jiang, and Daqing Zhang. 2019. Towards a Diffraction-based Sensing Approach on Human Activity Recognition. *Proceedings of the ACM on Interactive, Mobile, Wearable and Ubiquitous Technologies* 3, 1 (2019), 33.

[47] Fusang Zhang, Daqing Zhang, Jie Xiong, Hao Wang, Kai Niu, Beihong Jin, and Yuxiang Wang. 2018. From Fresnel Diffraction Model to Fine-Grained Human Respiration Sensing with Commodity Wi-Fi Devices. *Proceedings of the ACM on Interactive, Mobile, Wearable and Ubiquitous Technologies* 2, 1 (2018), 1–23.